An Implicit Pressure Correction Method for Incompressible Navier-Stokes Equations on Unstructured Cartesian Grids

Dartzi Pan

Institute of Aeronautics and Astronautics, National Cheng Kung University
Tainan, Taiwan ROC
Email: dpan@mail.ncku.edu.tw

ABSTRACT

An implicit pressure correction method on unstructured Cartesian grid is developed for the incompressible Navier-Stokes equations. An immersed boundary method is also incorporated to treat the body geometry. The pressure Poisson equation is solved by a multi-grid method. A fourth order artificial dissipation is added to the pressure field to suppress the even-odd decoupling. Tests show that with an appropriate amount of dissipation, the method is second order accurate both in time and space. The driven cavity flows with and without immersed bodies are computed to demonstrate the capability of the present scheme.

Keyword: *Implicit Pressure Correction Method, Unstructured Cartesian Grids, Immersed Boundary Method*

1. Introductions

The numerical method for the incompressible Navier-Stokes equations has been highly developed in recent years. One popular method is the pressure correction method (or fractional step method) [1-5] in which the divergence-free condition is obtained via an appropriate pressure field. In these methods the velocity is updated by a 2-step predictor-corrector time integration. In the predictor step the intermediate velocity field computed from the momentum equations is usually not divergence free. Then in the corrector step a pressure field is applied to correct the non-divergence-free part of the intermediate velocity. This pressure field obeys a Poisson equation. Normally in these methods staggered grids are used to achieve pressure-velocity coupling [1-3]. If a non-staggered grid is used, then a cell-face velocity is defined in addition to the cell-center variables [4,5] to compute the volume flux. The time integration method used for velocity is usually semi-implicit. That is, the predictor step of the time integration usually employs an explicit scheme (Adams-Bashforth or RK3) for the inviscid terms and an implicit scheme (Trapezoidal rule) for the viscous terms. It is well known that the RK3 scheme has a CFL limit of $\sqrt{3}$ and the Adams-Bashforth scheme is weakly unstable for the model convection equation [1]. These stability limitations may become sever when the grid is locally refined or stretched.

Traditionally a body-fitted [1,5] structured or unstructured grid system is employed to handle the immersed bodies in the flow field. More recently the immersed boundary method [2,3,4] on fixed Eulerian grids has gained popularity for their ease in treating the complex geometries. In Fadlun et al. [2] and Kim et al. [3], a body in the flow field is modeled by adding momentum forcing to the appropriate grid cells to simulate the appropriate boundary condition. In Mittal et al. [4], the grid cells cut by the body are treated with special differencing schemes. The usefulness of these methods lies on the appropriateness and simplicity of the procedure to model the true body geometry and its effects on the flow field. In this aspect, the capability of local refinement around body boundaries is desirable.

In this work an implicit pressure correction method is developed to solve the incompressible Navier-Stokes equations. The fully implicit time integration is achieved by the technique of sub-iteration [6]. The unstructured Cartesian grid system is employed to allow local refinement when necessary. The pressure Poisson equation is solved by an implicit multi-grid method [7]. A fourth order artificial dissipation is added to the pressure field to suppress the even-odd decoupling of pressure. An immersed boundary method is also developed to handle the immersed bodies. The no-slip boundary condition is enforced by the method of direct forcing [2]. The driven cavity flows with

Report Documentation Page

Public reporting burden for the collection of information is estimated to average 1 hour per response, including the time for reviewing instructions, searching existing data sources, gathering and maintaining the data needed, and completing and reviewing the collection of information. Send comments regarding this burden estimate or any other aspect of this collection of information, including suggestions for reducing this burden, to Washington Headquarters Services, Directorate for Information Operations and Reports, 1215 Jefferson Davis Highway, Suite 1204, Arlington VA 22202-4302. Respondents should be aware that notwithstanding any other provision of law, no person shall be subject to a penalty for failing to comply with a collection of information if it does not display a currently valid OMB control number.

1. REPORT DATE **14 APR 2005**	2. REPORT TYPE **N/A**	3. DATES COVERED **-**

4. TITLE AND SUBTITLE	5a. CONTRACT NUMBER
An Implicit Pressure Correction Method for Incompressible Navier-Stokes Equations on Unstructured Cartesian Gridsrbine	5b. GRANT NUMBER
	5c. PROGRAM ELEMENT NUMBER

6. AUTHOR(S)	5d. PROJECT NUMBER
	5e. TASK NUMBER
	5f. WORK UNIT NUMBER

7. PERFORMING ORGANIZATION NAME(S) AND ADDRESS(ES)	8. PERFORMING ORGANIZATION REPORT NUMBER
Institute of Aeronautics and Astronautics, National Cheng Kung University Tainan, Taiwan ROC	

9. SPONSORING/MONITORING AGENCY NAME(S) AND ADDRESS(ES)	10. SPONSOR/MONITOR'S ACRONYM(S)
	11. SPONSOR/MONITOR'S REPORT NUMBER(S)

12. DISTRIBUTION/AVAILABILITY STATEMENT
Approved for public release, distribution unlimited

13. SUPPLEMENTARY NOTES
See also ADM001800, Asian Computational Fluid Dynamics Conference (5th) Held in Busan, Korea on October 27-30, 2003. , The original document contains color images.

14. ABSTRACT

15. SUBJECT TERMS

16. SECURITY CLASSIFICATION OF:			17. LIMITATION OF ABSTRACT	18. NUMBER OF PAGES	19a. NAME OF RESPONSIBLE PERSON
a. REPORT **unclassified**	b. ABSTRACT **unclassified**	c. THIS PAGE **unclassified**	**UU**	**8**	

immersed bodies are computed to demonstrate the capability of the present scheme.

2. Implicit Pressure Correction Method

The integral form of incompressible Navier-Stoked equations can be written as

$$\oint_{CS} \vec{v} \cdot d\vec{S} = 0.$$

$$\int_{CV} \frac{\partial}{\partial t} \vec{v} dV = -\left(\oint_{CS} \vec{v}\vec{v} \cdot d\vec{S} - \frac{1}{Re} \oint_{CS} \vec{\nabla} \vec{v} \cdot d\vec{S} + \oint_{CS} P d\vec{S} + \vec{f}_B \right)$$

$$= -\left(\vec{R} + \oint_{CS} P d\vec{S} + \vec{f}_B \right)$$

(1)

where $\vec{v}$ and P are Cartesian velocity and pressure, Re is Reynolds number, $\vec{f}_B$ is the momentum forcing simulating the solid body, V is the volume of the control volume CV, $\vec{S}$ is the surface CS of the cell, $\vec{R}$ represents the surface integral of inviscid and viscous fluxes except the pressure term. Assume that the flow state at time level n is known on a cell-centered non-stagger grid. An implicit time integration with sub-iteration [6] applied to the momentum equation can be written as:

$$\left(\frac{\Delta V}{\Delta t} + \boldsymbol{q} \frac{\partial \vec{R}}{\partial \vec{v}} + \frac{\partial \vec{f}_B}{\partial \vec{v}} \right) (\vec{v}^{s+1} - \vec{v}^s) =$$

$$- \left(\frac{\vec{v}^s - \vec{v}^n}{\Delta t} \Delta V + \boldsymbol{q} (\vec{R}^s + \sum_{CS} P^m \Delta \vec{S}) + (1 - \boldsymbol{q})(\vec{R}^n + \sum_{CS} P^n \Delta \vec{S}) + \vec{f}_B \right)$$

(2)

where the superscript n is the time level index, s is the sub-iteration index for velocity, m is the sub-iteration index for pressure, Δt is the time increment, ΔV is the cell volume, $\Delta \vec{S}$ is the cell face, the summation operator represents a closed surface integral over the cell faces, and $0 \le \boldsymbol{q} \le 1$. Equation (2) is iterated in s with fixed m and n. The initial conditions are $P^m = P^n$ at $m=1$ and $\vec{v}^s = \vec{v}^n$ at $s=1$. When the sub-iteration in s converges, we obtain an intermediate state $\vec{v}^*$ satisfying

$$\frac{\vec{v}^* - \vec{v}^n}{\Delta t} \Delta V + \boldsymbol{q} (\vec{R}^* + \sum_{CS} P^m \Delta \vec{S}) + (1 - \boldsymbol{q})(\vec{R}^n + \sum_{CS} P^n \Delta \vec{S}) + \vec{f}_B = 0$$

(3)

Generally this $\vec{v}^*$ does not satisfy the divergence-free condition. A pressure correction is sought to obtain a divergence-free velocity $\vec{v}^{m+1}$ and pressure P^{m+1} that satisfy the following equations:

$$\frac{\vec{v}^{m+1} - \vec{v}^n}{\Delta t} \Delta V + \boldsymbol{q} (\vec{R}^* + \sum_{CS} P^{m+1} \Delta \vec{S}) + (1 - \boldsymbol{q})(\vec{R}^n + \sum_{CS} P^n \Delta \vec{S}) + \vec{f}_B = 0.$$

$$Div(\vec{v}^{m+1}) = 0.$$

(4)

where $Div(\bullet)$ represents an appropriate divergence operator. Set the pressure correction as $\boldsymbol{f} = P^{m+1} - P^m$ and subtract Eq. (3) from Eq. (4), we obtain the equation for velocity correction:

$$\frac{\vec{v}^{m+1} - \vec{v}^*}{\Delta t} + \boldsymbol{q} \frac{1}{\Delta V} \sum_{CS} \boldsymbol{f} \Delta \vec{S} = 0$$

(5)

Take the divergence of Eq. (5), we obtain the Poisson equation for the pressure correction:

$$Div\left(\frac{1}{\Delta V} \sum_{CS} \boldsymbol{f} \Delta \vec{S} \right) = \frac{1}{\boldsymbol{q} \Delta t} Div(\vec{v}^*)$$

(6)

Equation (6) is to be solved for $\boldsymbol{f}$ and the pressure P^{m+1}, which in turn is to be substituted into Eq. (5) to obtain the divergence-free velocity $\vec{v}^{m+1}$. Equations (2), (5) and (6) constitute one pressure iteration in m. This iteration in m is considered converged when the pressure and velocity corrections in Eq. (5) are small enough. When this is achieved, the latest computed flow field is the flow state at

the new time level $n+1$, that is, $\vec{v}^{n+1} = \vec{v}^{m+1} = \vec{v}^*$ and $P^{n+1} = P^{m+1} = P^m$. In this work, Eq. (2) is inverted by an approximate LU factorization scheme [6].

3. Poisson Equation and Cell-Face Velocity

To evaluate the fluxes, the variable values at the cell faces need to be reconstructed. First, the cell-vertex values are obtained by a distance-weighted averaging of the surrounding cell-center values. The averaging constant is proportional to the inverse of the distance from the cell center to the particular vertex. The variable gradients can be estimated by differencing the cell-vertex values enclosing the particular cell. Then the left and right states at a cell face can be linearly interpolated using the gradient just obtained. The mean cell-face velocity and pressure are obtained by a simple averaging of the left and right states:

$$\vec{v}_{f,mean} = 0.5(\vec{v}_f^L + \vec{v}_f^R), \qquad P_{f,mean} = 0.5(P_f^L + P_f^R) \tag{7}$$

where the superscript L and R respectively indicate the left and right states of a face, the subscript f indicates a cell face, the subscript *mean* indicates the mean values. The mean cell-face pressure is used to compute the surface integral of pressure in Eq. (2). This is equivalent to a central differencing for the pressure gradient on a Cartesian mesh. The mean cell-face velocity $\vec{v}_{f,mean}^*$ is used to compute the divergence of $\vec{v}^*$ in Eq. (6). This is equivalent to a central differencing for the divergence operator.

The left hand side operator of Eq. (6) is equivalent to a discretized Laplacian. However, it becomes non-compact when the divergence operator is applied, making the inversion of Eq. (6) expensive. Thus, for computational efficiency the left hand side of Eq. (6) is simplified as

$$\frac{1}{\Delta V} \sum_{CS} \bar{\nabla} \boldsymbol{f} \cdot \Delta \vec{S} = \frac{1}{\boldsymbol{q}\Delta t} \left(\frac{1}{\Delta V} \sum_{CS} \vec{v}_{f,mean}^* \cdot \Delta \vec{S} \right) \tag{8}$$

The left hand side operator is a compact Laplacian discretization when the cell-face $\bar{\nabla} \boldsymbol{f}$ is obtained by differencing the neighboring cell-center values. In this work, Eq. (8) is solved by a multi-grid method on unstructured Cartesian grid [7].

Note that Eq. (5) is an equation for cell-center velocities while the pressure at cell faces are interpolated. But Eq. (8) is an equation for cell-centered $\boldsymbol{f}$ with $\vec{v}_{f,mean}^*$ interpolated. Because of this inconsistency in variable locations, the cell-center $\vec{v}^{m+1}$ computed by Eq. (5) may not satisfy the divergence-free condition exactly. We resolve this inconsistency in a way similar to the approach in Ref. [4,5], by defining a new cell-face velocity. That is, while Eq. (5) is still used to update the cell-center velocity $\vec{v}^{m+1}$, a cell-face velocity $\vec{v}_f^{m+1}$ is updated from $\vec{v}_{f,mean}^*$ by

$$\frac{\vec{v}_f^{m+1} - \vec{v}_{f,mean}^*}{\Delta t} + \boldsymbol{q}\bar{\nabla} \boldsymbol{f} = 0 \tag{9}$$

where $\bar{\nabla} \boldsymbol{f}$ at the cell face f is obtained by differencing the neighbouring cell-center values. It is easy to verify that Eq. (9) is consistent with Eq. (8) and consequently $\vec{v}_f^{m+1}$ satisfies the divergence-free condition. This $\vec{v}_f^{m+1}$ is used to compute the volume flux at the next iteration in m. The face-center $\vec{v}_f^{m+1}$ is updated in parallel to the cell-centered $\vec{v}^{m+1}$, while the flow states are still the cell-center $\vec{v}^{m+1}$ and P^{m+1}.

3. Convective and Viscous Fluxes

When iterating Eq. (2) in s, the last past divergence-free velocity $\vec{v}_f^m$ is used to compute the volume flux. Thus, the convective momentum fluxes in $\vec{R}^s$ of Eq. (2) are computed as:

$$\vec{R}_{inv}^s = \sum_{CS} \begin{bmatrix} u^s \\ v^s \end{bmatrix}_{L/R} \vec{v}_f^m \cdot \Delta \vec{S} \tag{10}$$

where the subscripts L/R represents the velocity upwinding:

$$(\bullet)_{L//R} = \begin{cases} (\bullet)^L & if \quad \vec{v}_f^m \cdot \Delta\vec{S} > 0 \\ (\bullet)^R & if \quad \vec{v}_f^m \cdot \Delta\vec{S} \le 0 \end{cases} \tag{11}$$

Equation (10) is equivalent to a second-order accurate upwind differencing for the convective momentum fluxes. The viscous fluxes in $\vec{R}^s$ of Eq. (2) are computed as

$$\vec{R}_{vis}^s = \frac{1}{Re}\sum_{CS}\begin{bmatrix}\bar{\nabla}u^s\\\bar{\nabla}v^s\end{bmatrix}\cdot\Delta\vec{S} \tag{12}$$

The gradient of velocity components at the cell faces can be obtained by differencing the neighbouring cell-center values. On a regular Cartesian grid this is equivalent to a compact second-order accurate central differencing for the viscous terms.

5. Artificial Dissipation

Our experience indicates that the velocity upwinding and the use of $\bar{v}_f^m$ to compute the convective fluxes are not enough to prevent the even-odd decoupling of the pressure field. Thus, an artificial dissipation is added explicitly for stabilization. The dissipation for a cell is defined as

$$F^{disp} = \frac{cdisp}{1 + \Delta x / Re}\sum_{CS}(P_f^R - P_f^L)\hat{n}\cdot\hat{e} \tag{13}$$

where $\hat{n}$ is the unit normal of a cell face pointing outward of the cell, $\hat{e}$ is the Cartesian unit vector parallel to $\hat{n}$, and we take $0.01 \le cdisp \le 0.1$ in this paper. This dissipation is added explicitly to the pressure field after solving Eq. (8):

$$P^{m+1} = P^m + f + F^{disp} \tag{14}$$

It is easy to show that the dissipation is proportional to $\Delta x^4 \frac{\partial^4 p}{\partial x^4}$ for a Cartesian mesh. Our experience indicates that with an appropriate amount of *cdisp,* the added dissipation is beneficial and sometimes crucial to obtaining a smooth pressure distribution.

6. Order Analyses

All examples shown in this paper are computed on a personal computer using 32-bit single precision. The analytical solutions of decaying vortices [8] are used for order analyses:

$$u(x,y,t) = -\cos(a\mathbf{p}x)\sin(a\mathbf{p}y)e^{-2a^2\mathbf{p}^2t/Re}, \qquad v(x,y,t) = \sin(a\mathbf{p}x)\cos(a\mathbf{p}y)e^{-2a^2\mathbf{p}^2t/Re}$$

$$P(x,y,t) = -\frac{\cos(2a\mathbf{p}x) + \cos(2a\mathbf{p}y)}{4}e^{-4a^2\mathbf{p}^2t/Re}$$

Here we take $-8 \le x, y \le 8$, $a=1/8$, and $Re=1$. Exact solutions are used as initial and boundary conditions. The Trapezoidal rule with $q = 0.5$ is used for time integration. The iteration in m is considered adequate when both the L2 norms of divergence field and the pressure correction f are less than $1.\times 10^{-5}$ and at least one of the two is less than 0.5×10^{-5}. The allowable number of pressure iteration is set to $5 \le m \le 30$.

To test the spatial accuracy of the scheme, the system is integrated *48* time steps to *t=0.3* on Cartesian meshes of cell length Δx =0.125, 0.25 and *0.5*. The time step is $\Delta t = 0.00625$ to reduce the time discretization error. The constant *cdisp=0.03* is used. The L2 and maximum norms of the error in pressure and velocity are plotted in Fig. 1. The average order of accuracy estimated for pressure is *2.32* in L2 norms and *1.86* in maximum norms. For velocity, the accuracy is *2.03* in L2 norms and *2.27* in maximum norms. For comparison, similar curves are plotted for *cdisp=0* in Fig. 2. Without artificial dissipation in pressure, only the L2 norm of velocity has an average order of accuracy of *1.88*, all other norms deteriorate to first order or even worse. This has demonstrated the need for artificial dissipation in pressure.

To test the time accuracy, the system is integrated to *t=0.8* on a Cartesian grid with Δx =0.125. The time steps are Δt =0.2, 0.4 and 0.8. The maximum allowable number of pressure correction in *m* for each time step is increased to *1000*. The velocity and pressure norms verse time steps are plotted

in Fig. 3. The average order of accuracy for all norms in Fig. 3 is second order or higher. The maximum CFL number observed in the calculations for Fig. 3 is *6.4*. This indicates that the sub-iteration technique has eased the limitation on the time step.

7. Driven Cavity Flows

The numerical solutions of a driven cavity obtained by Ghia et al. [9] are used to test the steady-state computation of the present method. A Cartesian grid of size *128×128* is used to discretized a square cavity of unit length in size. The upper wall is moving to the right at unit speed. The Euler implicit method with $q = 1$ is used with $m \leq 1$ at each time step. We take *cdisp=0.01*. The Reynolds number *Re* is based on wall speed and the cavity width. For the case of *Re=3200*, the maximum CFL number is set to *2*. The velocity component *u(y)* along the vertical centerline and the velocity component *v(x)* along the horizontal centerline are plotted in Fig. 4. The comparison with the result of Ghia et al. [9] who also used a similar Cartesian grid is very good. The computed path lines are plotted in Fig. 5, showing one primary vortex at the center and three secondary vortices on the corners and the left wall.

8. Immersed Boundary Method

In this work, we use a level set function f_l defined on the cell vertices to track the presence of the immersed bodies. W chose f_l to be a signed distance function whose absolute value equals the shortest distance to the body surface. It is defined $f_l > 0$ outside the body, $f_l < 0$ inside, and $f_l = 0$ on the body surface. With f_l known, the volume fraction occupied by the immersed body in a cell, or the Volume of Body (VOB) function f_b, can be computed easily. We have $f_b = 1$ for body cells, $f_b = 0$ for fluid cells and $0 < f_b < 1$ for interface cells containing the body contour $f_l = 0$. We take $f_b = 0.5$ as the representative body surface. The accuracy of f_b depends on the assumed shape of the body contour of $f_l = 0$ inside the interface cells. Here we assume $f_l = 0$ contour is linear inside an interface cell. This simplifies the calculation of f_b, but the resulting f_b is only first-order accurate.

Assume that at any time level *n* the divergence-free body velocity $\vec{v}_b^n$ is known. For body cells with $f_b = 1$, the no-slip condition requires that $\vec{v} = \vec{v}_b^n$. For partially filled interface cells with $0 < f_b < 1$, special care must be taken to account for the influences of the body surface as accurately as possible. In Xiao [10], the cell-center velocity is defined as the volume average of the body velocity and the fluid velocity computed for the particular interface cell. In Fadlun et al. [2] and Kim et al. [3], the velocity of the interface cells is not computed by the flow equations but interpolated using the surrounding fluid and body cells. In our experience, both approaches will work when the immersed body is stationary. However, when the body is accelerating, an impulsive change in pressure will be created corresponding to the change in body velocity. Which approach can model this pressure change correctly requires further investigation efforts. Here, we show some results using the volume-averaging approach.

The direct momentum forcing in Eq. (2) is written as

$$\vec{f}_B = -f_b \left(\frac{\vec{v}_b - \vec{v}^n}{\Delta t} \Delta V + q(\bar{R}^s + \sum_{CS} P^m \Delta \bar{S}) + (1-q)(\bar{R}^n + \sum_{CS} P^n \Delta \bar{S}) \right) \qquad (15)$$

Thus, for fluid cells with $f_b = 0$, no forcing is applied. For body cells with $f_b = 1$, the converged solution of Eq. (2) is $\vec{v}^* = \vec{v}_b$. For interface cells with $0 < f_b < 1$, the solution is a volume average of the body velocity $\vec{v}_b$ and the fluid velocity $\vec{v}_{fluid}$. However, the fluid velocity $\vec{v}_{fluid}$ is not explicitly computed. Instead, the volume-averaged $\vec{v}^*$ computed by Eq. (2) is used as the fluid velocity.

As for the corrections for velocity and pressure, we assume that Eqs. (5), (6), (8) and (9) are valid for interface cells. For body cells, there is no need for velocity correction. Furthermore, because the body velocity is assumed divergence free, it is reasonable to assume that inside the body cells the pressure correction satisfies Eq. (6) with a zero source term, or equivalently the Laplace equation. In

essence this is equivalent to treating the body as an incompressible fluid with prescribed velocity distribution, and hence it satisfies the same pressure correction equation as the fluid outside the body.

9. Driven Cavity With Centered Cylinders

A stationary circular cylinder of radius *0.21* is placed at the center of the driven cavity in the last example. The cylinder radius is arbitrarily chosen. The grid has one level of refinement around the cylinder, as shown in Fig. 6. The Reynolds number based on the wall speed and the cavity width is *1000*. The computed particle paths are plotted in Fig. 7. The contour of VOB function $f_b = 0.5$ is also plotted as the cylinder wall. The smoothness of the streamlines over the cylinder wall indicates that the treatment of the interface cells is effective in representing a curved surface. For comparison's sake, a multi-zone body-fitted flow solver [6] is used to solve the same problem on a 5-zone grid. The velocity component *u(y)* along the vertical centerline and *v(x)* along horizontal centerline are compared in Fig. 8. The lines are computed by the body-fitted method and the symbols are computed by the immersed boundary method. Because the Although some difference can be seen in the figure, but generally the shapes of the velocity profiles compare very well.

The pressure and viscous forced experienced by the cylinder are also compared. For the body-fitted method, the pressure and viscous stresses are integrated along the cylinder surface to obtain the forces. For the current method, the forces experienced by the body are obtained by

$$\bar{f}_{body} = \sum_{all} f_b (-\bar{\nabla}P + \frac{1}{Re}\nabla^2 \bar{v})\Delta V \qquad (16)$$

The body-fitted method obtained a pressure force of *(-0.4619E-2, -0.4418E-4)* and a viscous force of *(-0.1734E-2, 0.6231E-3)*. The current method obtained a pressure force of *(-0.4619E-2, -0.1995E-3)* and a viscous force of *(-0.1305E-2, 0.4773E-3)*. The pressure forces are in better agreement than the viscous forces are. This is not surprising, since the immersed boundary method mainly influences the velocity profile near body surfaces and the pressure force is mainly an inviscid effect.

10. Conclusions

An implicit pressure correction method for the incompressible Navier-Stokes equations on unstructured Cartesian grid is developed and tested. The technique of sub-iteration is used to derive the implicit time integration equation. The pressure Poisson equation is solved by an implicit multi-grid method. A forth-order dissipation is added to the pressure field to control the even-odd decoupling. Tests show that with an appropriate amount of artificial dissipation, the present method is second-order accurate both in time and space. An immersed boundary method is also developed and tested. The results indicate that the current method is simple and effective in modeling the stationary immersed bodies. The extended use of the present approach to moving bodies is currently undergoing.

Acknowledgement

References

[1] Rai, M.M., "Direct Simulations of Turbulent Flow Using Finite-Difference Schemes", *J. Comput. Phys.* Vol. 96, (1991), pp.15-53.

[2] Fadlun, E.A., Verzicco, R., Orlandi, P. and Mohd-Yusof, J., "Combined Immersed-Boundary Finite-Difference Methods for Three-Dimensional Complex Flow Simulations", *J. Comput. Phys*, Vol. 161, (2000), pp. 35-60.

[3] Kim, J., Kim, D., and Choi, H., "An Immersed-Boundary Finite-Volume Method for Simulations of Flow in Complex Geometries", *J. Comput. Phys.*, Vol. 171, (2001), pp. 132-150.

[4] Ye, T., Mittal, R., Udaykumar, H.S. and Shyy, W., "An Accurate Cartesian Grid Method for Viscous Incompressible Flows with Complex Immersed Boundaries", *J. Comput. Phys.*, Vol. 156, (1999), pp. 209-240.

[5] Zang, Y., Street, R. L., and Koseff, J. R., "A Non-staggered Grid, Fractional Step Method for Time-Dependent Incompressible Navier-Stokes Equations in Curvilinear Coordinates," *J. Comput. Phys.*, Vol. 114, (1994), pp. 18-33.

[6] Pan, D. and Chang, C.H., "The Capturing of Free Surfaces in Incompressible Multi-Fluid Flows", *International Journal For Numerical Methods In Fluids*, Vol. 33, (2000), pp. 203-222.

[7] Pan, D., "An Unstructured Cartesian Poisson Solver," Proceedings of The 9th National Computational Fluid Dynamics Conference, Aug. 2002, Tainan, Taiwan ROC

[8] Ethier, C. R. and Steinman, D.A., "Exact Fully 3D Navier-Stokes Solutions for Benchmarking", *Int. J. Num. Met. Flu.,* Vol. 19, (1994), pp. 368-375.

[9] Ghia, U., Ghia, K.N. and Shin, C.T., "High-Re Solutions for Incompressible Flow Using the Navier-Stokes Equations and a Multigrid Method", *J. Comput. Phys.*, Vol. 48, (1982), pp. 387-411.

[10] Xiao, F., "A Computational Model for Suspended Large Rigig Bodies in 3D Unsteady Viscous Flows," *J. Comput. Phys.*, Vol. 155, (1999), pp. 348-379.
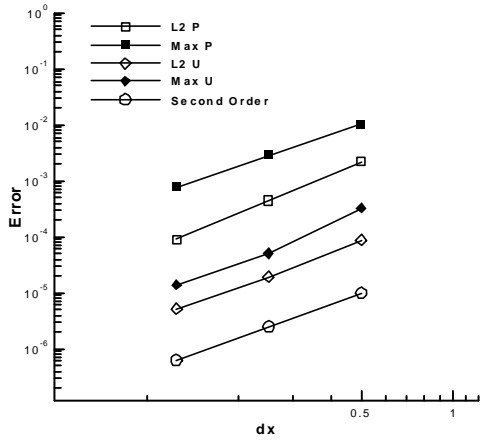
Fig. 1 Spatial accuracy test, decaying vortices, *cdisp=0.03*
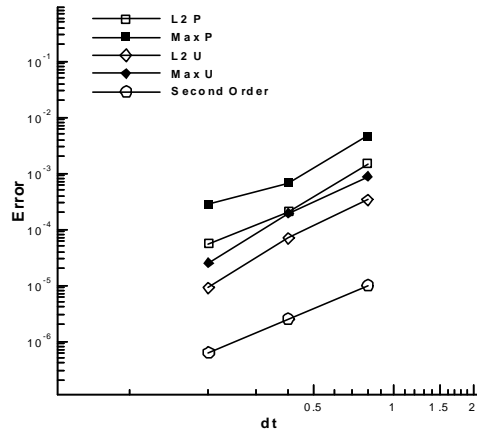
Fig. 3 Time accuracy test, decaying vortices, *q* =0.5
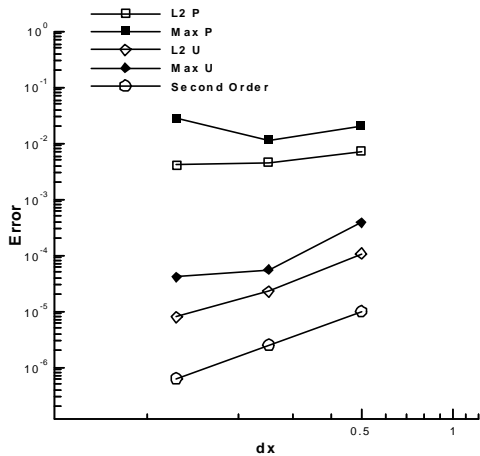
Fig. 2 Spatial accuracy test, decaying vortices, *cdisp=0.*
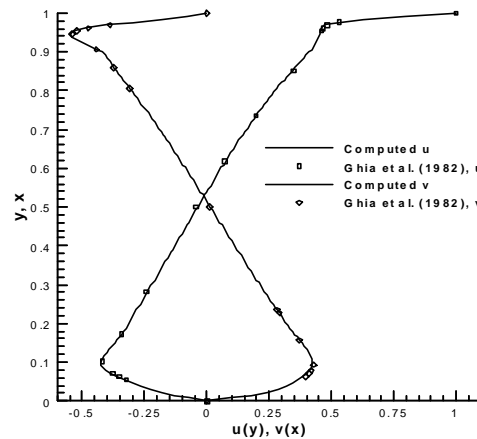
Fig. 4 Driven Cavity, *u(y)* along *x=0.5* and *v(x)* along *y=0.5, Re=3200, cdisp=0.01*
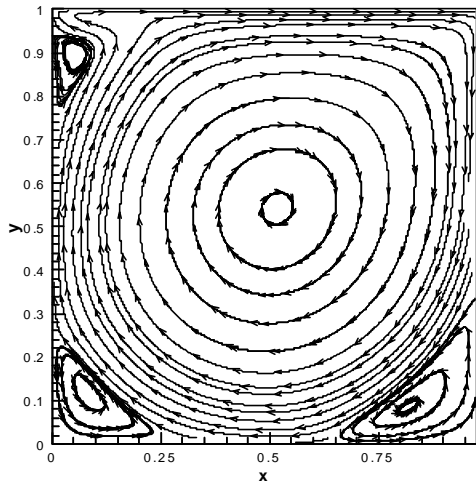
Fig. 5 Particle paths, *Re=3200*
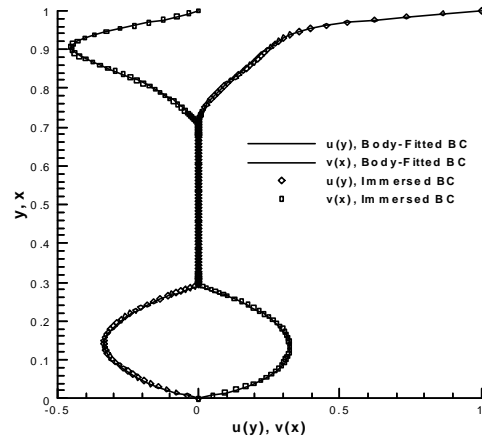
Fig. 8 Velocity *u(y)* along *x=0.5* and *v(x)* along *y=0.5,* driven cavity with centered cylinder
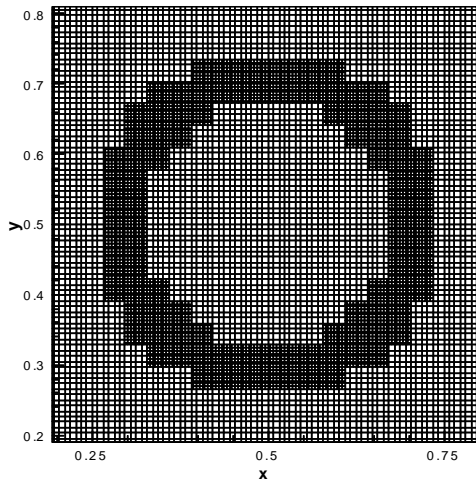

Fig. 6 Unstructured Cartesian grid for cavity with embedded cylinder, one level refinement
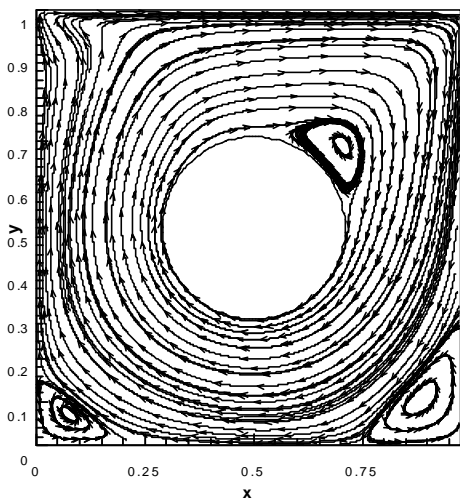
Fig. 7 Particle Paths for driven cavity with centered cylinder, *Re=1000*